Republic of Iraq

Ministry of Higher Education and Scientific Research
Hilla College, \ National University
Department of Medical Physics

Rrole of computed tomography in evaluation of brain tumor

The Department of Medical Physics at Al-Hilla University College, which is part of the requirements for obtaining a bachelor's degree in medical physics

A project Submitted by:

Abeas Ahmed
Afnan Hussain
Athrae jawad
Mansur Samawi
Mustafa Ali
Noor Al Huda Qasim
4th Grade Student

Supervisor
MS.C. Mohsen Hammoud

2024 **1445**

بسم الله الرحمن الرحيم



صدق الله العظيم

اهـــــــداء

إلى من لا يضاهيهما أحد في الكون، إلى من أمرنا الله ببرّهما ، إلى من بذلا الكثير ، وقدّما ما لا يمكن أن يردّ، إليكما تلك الكلمات اهلنا .....،

نهدي لكما هذا البَحث؛ فقد كنتم خير داعم لنا طوال مسيرتنا الدراسية .

الى استاذتنا و قدوتنا في كيفية تحقيق أهدافنا . أشكركم على نصائحك القيِّمة وثقتك في امكانياتنا

الشكر والتقدير

قال تعالى ولا أن شكرتم لأزيدنكم

قال رسول الله صلى الله عليه وآله وسلم من لم يشكر الناس لم يشكر الله عز وجل

أحمد الله تعالى حمدا كثيرا طيبا مباركا ملء السماوات والأرض على ما اكرمنا به

ثم نتوجه بجزيل الشكر وعظيم الامتنان

الى مشرفنا الاستاذ م.م. محسن حمود حفظه الله و أطال الله عمره لتفضله الكريم

بالإشراف على هذه الدراسة وتكرمه بنصحنا وتوجيه حتى أتمم هذه الدراسة

الى جميع اساتذتي الكرام

Contents

Title	Pag. No.
Chapter one \ Introduction	
Introduction	**1**
Types of Brain Tumors	**5**
Imaging Modalities	**6**
MRI	**7**
CT	**11**
PET	**12**
SPECT	**13**
Ultrasound	**13**
Classification and Segmentation Method	**14**
Classification Methods	**14**
MRI Brain Tumor Classification Using ML	**14**
X-rays	**27**
uses	**27**
The aim of study	**28**
Chapter Two \ literature review	
literature review	**33 -31**
Chapter three \ Patient and materials	
CT scan room design	**34**
Generator	**34**
X-ray tube	**35**
Filtration	**35**
Collimators.	**35**
GoldSeal Certified GE LightSpeed RT Series	**36**
Benefits.	**37**
Technology	**37**
Specifications	**37**
GoldSeal Advantage	**37**
Chapter four \ Discussion	
Discussion	**44**
Conclusion	**45**
References	**47**

Tables

Title	Pag. No.
.Table 1. Types of brain tumors	**6**
.Table 2. Properties of various MRI sequences	**10**
.Table 3. MRI brain tumor classification using ML	**18**
.Table 4. MRI brain tumor classification using DL	**26**

figure

Title	Pag. No.
Figure 1. Healthy brain MRI image showing white matter (WM), gray matter (GM), and .CSF	**8**
Figure 2. Fundamental MRI planes: (a) coronal, (b) sagittal, .and (c) axial	**9**
Figure 3. MRI brain tumor: (a) FLAIR image, (b) T1 image, and (c) T2 image	**10**
.Figure 4. CT brain tumor	**11**
.Figure 5. PET brain tumor	**12**
Figure 6 CAD method based on .ensemble classifiers	**15**
Figure 7. A block schematic showing the suggested approach. Reprinted (adapted) with permission from	**19**
Figure 8. Proposed method. Reprinted (adapted) with permission from .	**20**
Figure 9 Workflow of the suggested active learning framework based on transfer learning. Reprinted (adapted) with permission from	**21**
Figure 10. Proposed process for deep transfer learning. Reprinted (adapted) with permission from	**23**
Figer (11) images from a CT scan	**36**
Figer (12) A collection of images from a CT .scan with images of a brain scan	**38**

Abstract

Most of the components of the CT scan device are located inside the gantry. In addition to the gantry, the CT scan device also consists of an examination table and a control room. The design of CT scan rooms is usually similar, in that the examination table and gantry are in a room, while the control room is outside behind a lead barrier to protect against radiation.

In the control room there is a special computer that the radiology technician works on at the time of imaging, and part of the wall must be a window made of lead-equivalent glass so that we can see inside the room to intervene in the event of any emergency. The entrance for patients is different from the entrance for radiology technicians for several reasons, the most important of which are: protection from infection and so that it cannot be opened from the outside to ensure that no one enters at the time of radiation. It must also be a wide entrance to suit the patients' beds. It is important to have a waiting room and a changing room, and it is also possible to provide lockers for patients' belongings.

Radiotherapy simulation and planning demand the accuracy and precision of CT systems like the LightSpeed RT family. GoldSeal LightSpeed RT4 and RT16 systems help you image small structures, and see fine details for accurate contouring, and accurately detect edges of tumors in motion. The result is an effective balance of resolution, coverage, speed and dose for radiation therapy simulation at its best.

Chapter one

Introduction

Introduction

The human brain, which serves as the control center for all the body's organs, is a highly developed organ that enables a person to adapt to and withstand various environmental situations [1]. The human brain allows people to express themselves in words, carry out activities, and express thoughts and feelings. Cerebrospinal fluid (CSF), white matter (WM), and gray matter (GM) are the three major tissue components of the human brain. The gray matter regulates brain activity and comprises neurons and glial cells. The cerebral cortex is connected to other brain areas through white matter fibers comprising several myelinated axons. The corpus callosum, a substantial band of white matter fibers, connects the left and right hemispheres of the brain [2]. A brain tumor is a brain cell growth that is out of control and aberrant. Any unanticipated development may affect human functioning since the human skull is a rigid and volume-restricted structure, depending on the area of the brain involved. Additionally, it might spread to other organs, further jeopardizing human functions [3]. Early cancer detection makes the ability to plan effective treatment possible, which is crucial for the healthcare sector [4]. Cancer is difficult to cure, and the odds of survival are significantly reduced if it spreads to nearby cells. Undoubtedly, many lives could be preserved if cancer was detected at its earliest stage using quick and affordable diagnostic methods. Both invasive and noninvasive approaches may be utilized to diagnose brain cancer. An incision is made during a biopsy to extract a lesion sample for analysis. It is regarded as the gold standard for the diagnosis of cancer, where pathologists examine several cell characteristics of the tumor specimen under a microscope to verify the malignancy.

Noninvasive techniques include physical inspections of the body and imaging modalities employed for imaging the brain [5]. In comparison to brain biopsy, other imaging modalities, such as CT scans and MRI images, are more rapid and secure. Radiologists use these imaging techniques to identify brain problems, evaluate the development of diseases, and plan surgeries [6]. However, brain scans or image interpretation to diagnose illnesses are prone to inter-reader variability and accuracy, which depends on the medical practitioner's competency [5]. It is crucial to accurately identify the type of brain disorder to reduce diagnostic errors. Utilizing computer-aided diagnostic (CAD) technologies can improve accuracy. The fundamental idea behind CAD is to offer a computer result as an additional guide to help radiologists interpret images and shorten the reading time for images. This enhances the accuracy and stability of radiological diagnosis [7]. Several CAT-based artificial intelligence techniques, such as machine learning (ML) and deep learning (DL), are described in this review for diagnosing tissues and segmenting tumors. The segmentation process is a crucial aspect of image processing. This approach includes a procedure for extracting the area that helps determine whether a region is infected. Using MRI images to segment brain tumors presents various challenges, including image noise, low contrast, loss borders, shifting intensities inside tissues, and tissue-type variation.

The most complex and crucial task in many medical image applications is detecting and segmenting brain tumors because it often requires much data and information. Tumors come in a variety of shapes and sizes. Automatic or semiautomatic detection/segmentation, helped by AI, is currently crucial in medical diagnostics. The medical professionals must authenticate the boundaries and areas of the brain cancer and ascertain where precisely it rests and the exact impacted locations before therapies such as chemotherapy, radiation, or brain

surgery. This review examines the output from various algorithms that are used in segmenting and detecting brain tumors.

The review is structured as follows: Types of brain tumors are described in Section 2. The imaging modalities utilized in brain imaging are discussed in Section 3. The review algorithms used in the study are provided in Section 4. A review of the relevant state-of-the-art is provided in Section 5. The review is discussed in Section 6. The work's conclusion is presented in Section 7.

2.1. Types of Brain Tumors

The main three parts of the brain are the brain stem, cerebrum, and cerebellum [1]. The cerebellum is the second-largest component of the brain and manages bodily motor activities, including balance, posture, walking, and general coordination of movements. It is positioned behind the brain and connected to the brain stem. Internal white matter, tiny but deeply positioned volumes of gray matter, and a very thin gray matter outer cortex can all be found in the cerebellum and cerebrum. The brainstem links to the spinal cord. It is situated at the brain's base. Vital bodily processes, including motor, sensory, cardiac, repositories, and reflexes, are all under the control of the brainstem. Its three structural components are the medulla oblongata, pons, and midbrain [2]. A brain tumor is the medical term for an unexpected growth of brain cells [8]. According to the tumor's location, the kind of tissue involved, and whether they are malignant or benign, scientists have categorized several types of brain tumors based on the location of the origin (primary or secondary) and additional contributing elements [9]. The World Health Organization (WHO) categorized brain tumors into 120 kinds. This categorization is based on the cell's origin and behavior, ranging from less aggressive to greater aggressive. Even certain tumor forms are rated, with grades I being the least malignant (e.g., meningiomas, pituitary tumors) and IV being the most malignant. Despite differences in grading systems that rely on the kind of tumor, this denotes the pace of growth [10]. The most frequent type of brain tumor in adults is glioma, which may be classified into HGG and LGG. The WHO further categorized LGG into I–II grade tumors and HGG into III–IV grade. To reduce diagnosing errors, accurate identification of the specific type of brain disorder is crucial for treatment planning. A summary of various types of brain tumors is provided in Table 1.

Table 1. Types of brain tumors.

Types of Tumors Based on	Type	Comment
Nature	Benign	Less aggressive and grows slowly
	Malignant	Life-threatening and rapidly expanding
Origin	Primary tumor	Originates in the brain directly
	Secondary tumor	This tumor develops in another area of the body like lung and breast before migrating to the brain
Grading	Grade I	Basically, regular in shape, and they develop slowly
	Grade II	Appear strange to the view and grow more slowly
	Grade III	These tumors grow more quickly than grade II cancers
	Grade IV	Reproduced with greater rate
Progression stage	Stage 0	Malignant but do not invade neighboring cells
	Stage 1	Malignant and quickly spreading
	Stage 2	
	Stage 3	
	Stage 4	The malignancy invades every part of the body

2.2. Imaging Modalities

For many years, the detection of brain abnormalities has involved the use of several medical imaging methods. The two brain imaging approaches are structural and functional scanning [11]. Different measurements relating to brain anatomy, tumor location, traumas, and other brain illnesses compose structural imaging [12]. The finer-scale metabolic alterations, lesions, and visualization of brain activity are all picked up by functional imaging methods. Techniques including CT, MRI, SPECT, positron emission tomography (PET), (FMRI), and ultrasound (US) are

utilized to localize brain tumors for their size, location as well as shape, and other characteristics [13].

2.3. MRI

MRI is a noninvasive procedure that utilizes nonionizing, safe radiation [14] to display the 3D anatomical structure of any region of the body without the need for cutting the tissue. To acquire images, it employs RF pulses and an intense magnetic field [15].

The body is intended to be positioned within an intense magnetic field. The water molecules of the human body are initially in their equilibrium state when the magnets are off. The magnetic field is then activated by moving the magnets. The body's water molecules align with the magnetic field's direction under the effect of this powerful magnetic field [14]. Protons are stimulated to spin opposing the magnetic field and realign by the application of a high RF energy pulse to the body in the magnetic field's direction. Protons are stimulated to spin opposing the magnetic field and realign by the application of a high RF energy pulse to the body in the magnetic field's direction. When the RF energy pulse is stopped, the water molecules return to their state of equilibrium and align with the magnetic field once more [14]. This causes the water molecules to produce RF energy, which the scanner detects and transforms into visual images [16]. The tissue structure determines the amount of RF energy the water molecules can use. As we can see in Figure 1, healthy brain has white matter (WM), gray matter (GM), and CSF, according to a structural MRI scan [17]. The primary difference between these tissues in a structural MRI scan is based on the amount of water they contain, with WM constituting 70% water and GM containing 80% water. The CSF fluid is almost entirely composed of water, as shown in Figure 1.

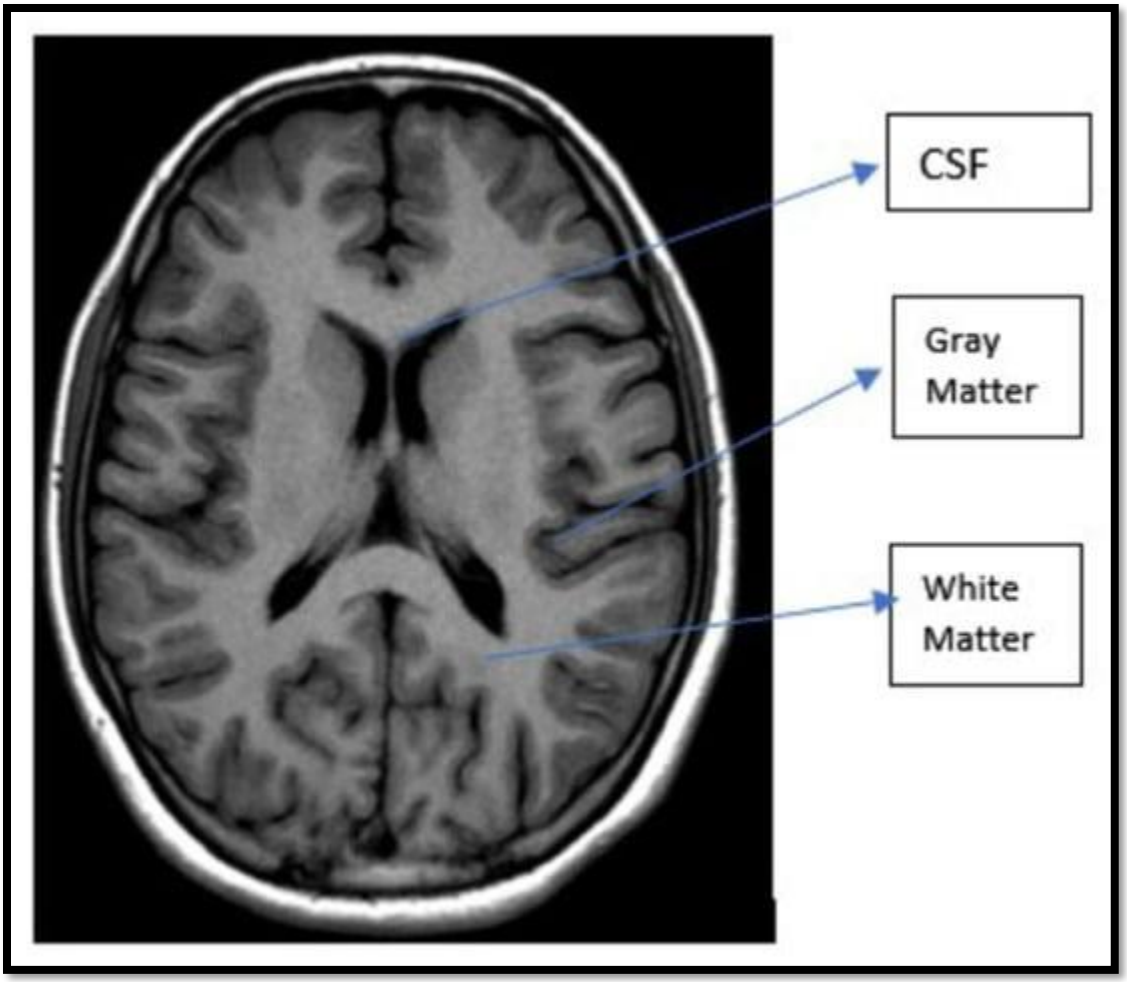

Figure 1. Healthy brain MRI image showing white matter (WM), gray matter (GM), and CSF [17].

Figure 2 illustrates the fundamental MRI planes used to visualize the anatomy of the brain: axial, coronal, and sagittal. Tl, T2, and FLAIR MRI sequences are most often employed for brain analysis [14]. A Tl-weighted scan can distinguish between gray and white matter. T2-weighted imaging is water-content sensitive and is therefore ideally suited to conditions where water accumulates within the tissues of the brain.

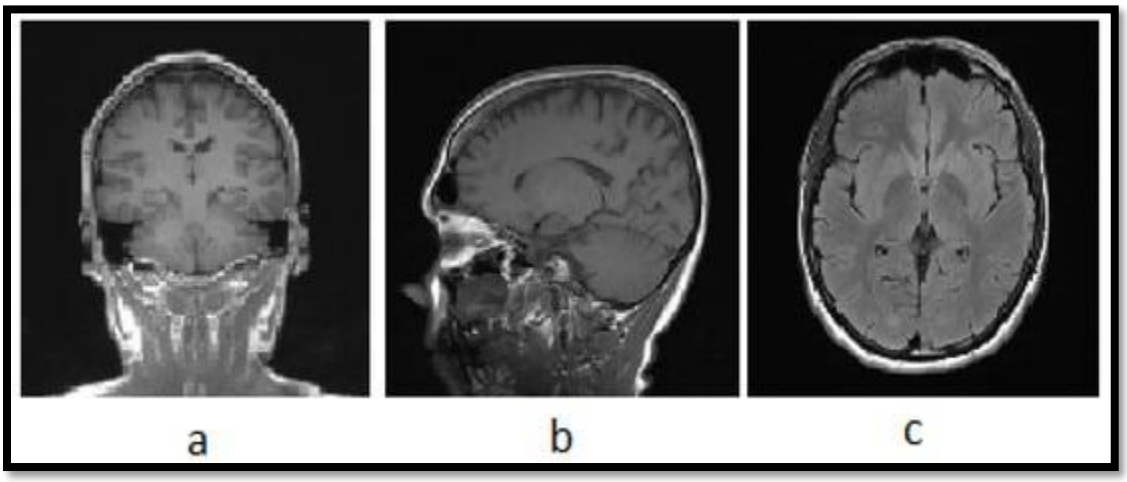

Figure 2. Fundamental MRI planes: (a) coronal, (b) sagittal, and (c) axial.

In pathology, FLAIR is utilized to differentiate between CSF and abnormalities in the brain. Gray-level intensity values in pixel spaces form an image during an MRI scan. The values of the gray-level intensity are dependent on the cell density. On T1 and T2 images of a tumor brain, the intensity level of the tumorous tissues differs [16]. The properties of various MRI sequences are shown in Table 2.

Table 2. Properties of various MRI sequences.

	T1	T2	Flair
White Matter	Bright	Dark	Dark
Gray Matter	Gray	Dark	Dark
CSF	Dark	Bright	Dark
Tumor	Dark	Bright	Bright

Most tumors show low or medium gray intensity on T1-w. On T2-w, most tumors exhibit bright intensity [17]. Examples of MRI tumor intensity level are shown in Figure 3.

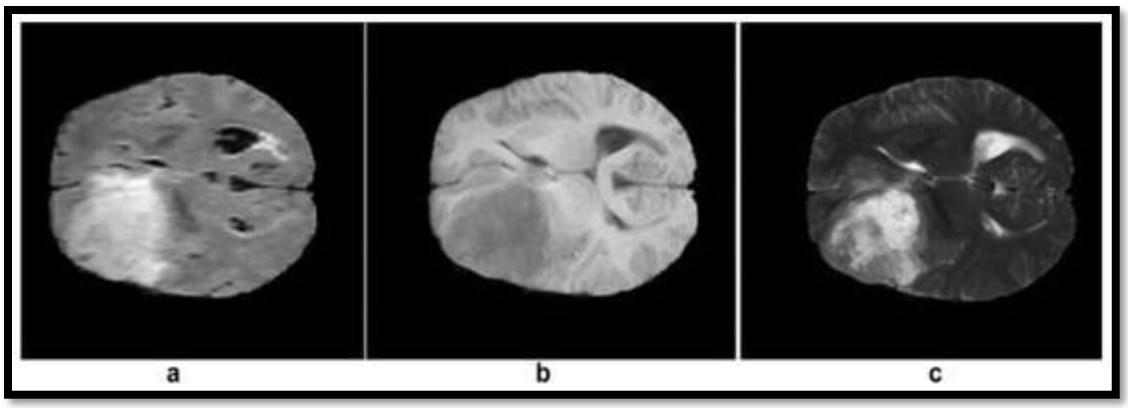

Figure 3. MRI brain tumor: (a) FLAIR image, (b) T1 image, and (c) T2 image [17].

Another type of MRI identified as functional magnetic resonance imaging (fMRI) [18] measures changes in blood oxygenation to interpret brain activity. An area of the brain that is more active begins to use more blood and oxygen. As a result, an fMRI correlates the location and mental process to map the continuing activity in the brain.

2.4. CT

CT scanners provide finely detailed images of the interior of the body using a revolving X-ray beam and a row of detectors. On a computer, specific algorithms are used to process the images captured from various angles to create cross-sectional images of the entire body [19]. However, a CT scan can offer more precise images of the skull, spine, and other bone structures close to a brain tumor, as shown in Figure 4. Patients typically receive contrast injections to highlight aberrant tissues. The patient may occasionally take dye to improve their image. When an MRI is unavailable, and the patient has an implantation like a pacemaker, a CT scan may be performed to diagnose a brain tumor. The benefits of using CT scanning are low cost, improved tissue classification detection, quick imaging, and more widespread availability. The radiation risk in a CT scan is 100 times greater than in a standard X-ray diagnosis [19].

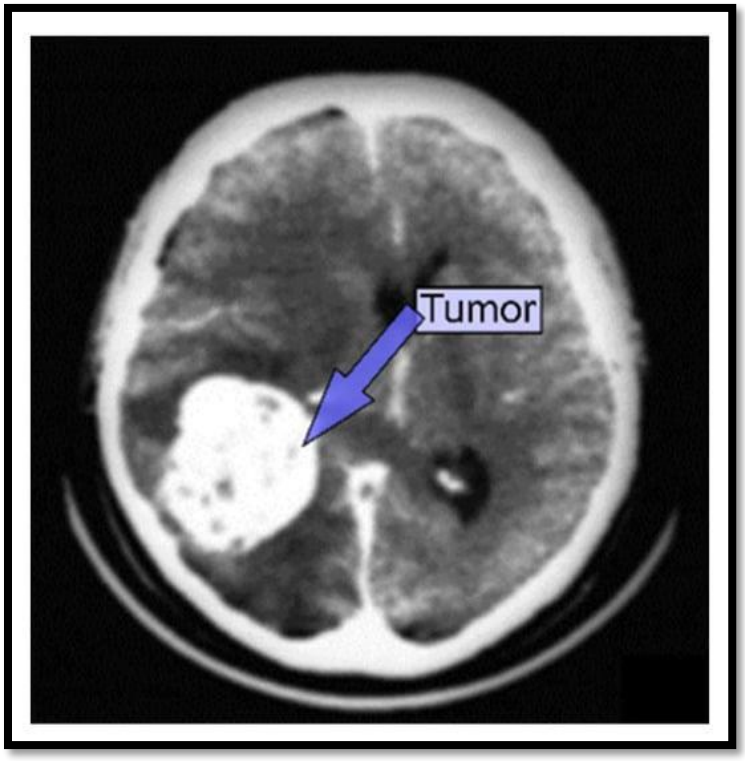

Figure 4. CT brain tumor.

2.5. PET

An example of a nuclear medicine technique that analyzes the metabolic activity of biological tissues is positron emission tomography (PET) [20]. Therefore, to help evaluate the tissue being studied, a small amount of a radioactive tracer is utilized throughout the procedure. Fluorodeoxyglucose (FDG) is a popular PET agent for imaging the brain. To provide more conclusive information on malignant (cancerous) tumors and other lesions, PET may also be utilized in conjunction with other diagnostic procedures like CT or MRI. PET scans an organ or tissue by utilizing a scanning device to find photons released by a radionuclide at that site [20]. The chemical compounds that are normally utilized by the specific organ or tissue throughout its metabolic process are combined with a radioactive atom to create the tracer used in PET scans, as shown in Figure 5.

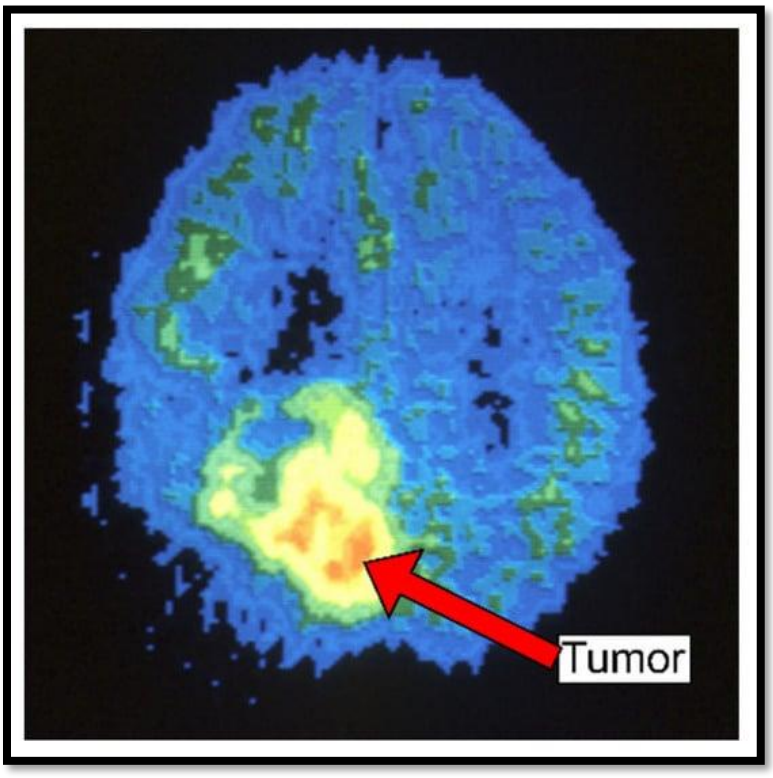

Figure 5. PET brain tumor.

2.6. SPECT

A nuclear imaging examination called a single-photon emission computed tomography (SPECT) combines CT with a radioactive tracer. The tracer is what enables medical professionals to observe the blood flow to tissues and organs [21]. A tracer is injected into the patient's bloodstream prior to the SPECT scan. The radiolabeled tracer generates gamma rays that the CT scanner can detect since it is radiolabeled. Gamma-ray information is gathered by the computer and shown on the CT cross-sections. A 3D representation of the brain can be created by adding these cross-sections back together [21].

2.7. Ultrasound

An ultrasound is a specialized imaging technique that provides details that can be useful in cancer diagnosis, especially for soft tissues. It is frequently employed as the initial step in the typical cancer diagnostic procedure [22]. One advantage of ultrasound is that a test can be completed swiftly and affordably without subjecting the patient to radiation. However, ultrasound cannot independently confirm a cancer diagnosis and is unable to generate images with the precise level of resolution or detail like a CT or MRI scan. A medical expert gently moves a transducer throughout the patient's skin across the region of the body being examined during a conventional ultrasound examination. A succession of high-frequency sounds is generated by the transducer, which "bounce off" the patient's interior organs. The ensuing echoes return to the ultrasound device, which then transforms the sound waves into a 2D image that may be observed in real-time on a monitor. According to [22], US probes have been applied in brain tumor resection. According to the degree of density inside the tissue being assessed, the shape and strength of ultrasonic echoes can change. An ultrasound can detect tumors that may

be malignant because solid masses and fluid-filled cysts bounce sound waves differently.

2.8. Classification and Segmentation Method

As was stated in the introduction, brain tumors are a leading cause of death worldwide. Computer-aided detection and diagnosis refer to software that utilizes DL, ML, and computer vision for analyzing radiological and pathological images. It has been created to assist radiologists in diagnosing human disease in various body regions, including applications for brain tumors. This review explored different CAT-based artificial intelligence approaches, including ML and DL, for automatically classifying and segmenting tumors.

2.9. Classification Methods

A classification is an approach in which related datasets are grouped together according to common features. A classifier in classification is a model created for predicting the unique features of a class label. Predicting the desired class for each type of data is the fundamental goal of classification. Deep learning and machine learning techniques are used for the classification of medical images. The key distinction between the two types is the approach for obtaining the features used in the classification process.

2.10.MRI Brain Tumor Classification Using ML

The automated classification of brain cancers using MRI images has been the subject of several studies. Cleaning data, feature extraction, and feature selection are the basic steps in the machine learning (ML) process that have been used for this purpose. Building an ML model based on labeled samples is the last step. A summary of MRI brain tumor classification using ML.

An NN-based technique to categorize a given MR brain image as either normal or abnormal is presented in [23]. In this method, features were first extracted from images using the wavelet transform, and then the dimensionality of the features was reduced using PCA methodology. The reduced features were routed to a back-propagation NN that uses a scaled conjugate gradient (SCG) to determine the best weights for the NN. This technique was used on 66 images, 18 of which were normal and 48 abnormal. On training and test images, the classification accuracy was 100%.

An automated and efficient CAD method based on ensemble classifiers was proposed by Arakeri and Reddy [24] for the classification of brain cancers on MRI images as benign or malignant. A tumor's texture, shape, and border properties were extracted and used as a representation. The ICA approach was used to select the most significant features. The ensemble classifier, consisting of SVM, ANN, and kNN classifiers, is trained using these features to describe the tumor. A dataset consisting of 550 patients' T1- and T2-weighted MR images was used for the experiments. With an accuracy of 99.09% (sensitivity 100% and specificity 98.21%), the experimental findings demonstrated that the suggested classification approach achieves strong agreement with the combined classifier and is extremely successful in the identification of brain tumors. Figure 6 illustrates the CAD method based on ensemble classifiers.

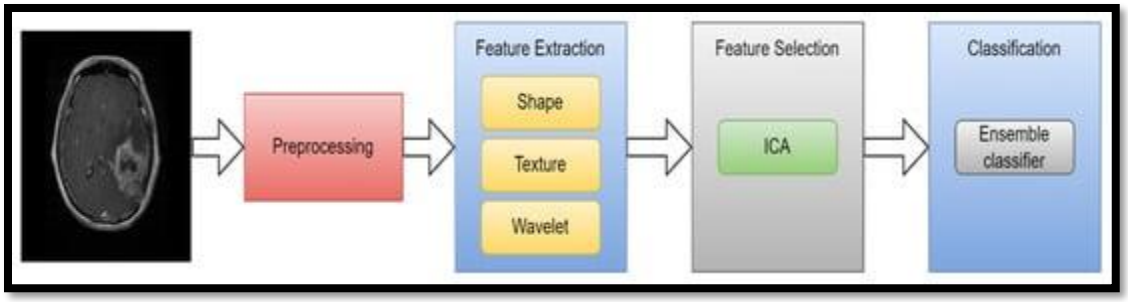

Figure 6 CAD method based on ensemble classifiers.

In [25], the authors suggested a novel, wavelet-energy-based method for automatically classifying MR images of the human brain into normal or abnormal. The classifier was SVM, and biogeography-based optimization (BBO) was utilized to enhance the SVM's weights. They succeeded in achieving 99% precision and 97% accuracy.

Amin et al. [26] suggest an automated technique to distinguish between malignant and benign brain MRI images. The segmentation of potential lesions has used a variety of methodologies. Then, considering shape, texture, and intensity, a feature set was selected for every candidate lesion. The SVM classifier is then used on the collection of features to compare the proposed framework's precision using various cross-validations. Three benchmark datasets, including Harvard, Rider, and Local, are used to verify the suggested technique. For the procedure, the average accuracy was 97.1%, the area under the curve was 0.98, the sensitivity was 91.9%, and the specificity was 98.0%.

A suitable CAD approach toward classifying brain tumors is proposed in [27]. The database includes meningioma, astrocytoma, normal brain areas, and primary brain tumors. The radiologists selected 20 × 20 regions of interest (ROIs) for every image in the dataset. Altogether, these ROI(s) were used to extract 371 intensity

and texture features. These three classes were divided using the ANN classifier. Overall classification accuracy was 92.43%.

Four hundred twenty-eight T1 MR images from 55 individuals were used in a varied dataset for multiclass brain tumor classification [28]. A based-on content active contour model extracted 856 ROIs. These ROIs were used to extract 218 intensity and texture features. PCA was employed in this study to reduce the size of the feature space. The ANN was then used to classify these six categories. The classification accuracy was seen to have reached 85.5%.

A unique strategy for classifying brain tumors in MRI images was proposed in [29] by employing improved structural descriptors and hybrid kernel-SVM. To better classify the image and improve the texture feature extraction process using statistical parameters, they used GLCM and histograms to derive the texture feature from every region. Different kernels were combined to create a hybrid kernel SVM classifier to enhance the classification process. They applied this technique to only axial T1 brain MRI images—93% accuracy for their suggested strategy.

A hybrid system composed of two ML techniques was suggested in [30] for classifying brain tumors. For this, 70 brain MR images overall (60 abnormal, 10 normal) were taken into consideration. DWT was used to extract features from the images. Using PCA, the total number of features was decreased. Following feature extraction, feed-forward back-propagation ANN and KNN were applied individually on the decreased features. The back-propagation learning method for updating weights is covered by FP-ANN. KNN has already been covered. Using KNN and FP-ANN, this technique achieves 97% and 98% accuracy, respectively [31].

A strategy for classifying brain MRI images was presented in [32]. Initially, they used an enhanced image improvement method that comprises two distinct steps: noise removal and contrast enhancement using histogram equalization. Then, using a DWT to extract features from an improved MR brain image, they further decreased these features by mean and standard deviation. Finally, they developed a sophisticated deep neural network (DNN) to classify the brain MRI images as abnormal or normal, and their strategy achieved 95.8%.

Table 3. MRI brain tumor classification using ML.

Ref.	Scan	Year	Feature Extraction	Feature Selection	Classification	Acc.
[96]	MRI	2010	GLCM	PCA	ANN and KNN	98% and 97%
[91]	MRI	2011	Wavelet	PCA	Back-propagation NN	100.00%
[94]	MRI	2013	Intensity and texture	PCA	ANN	85.50%
[95]	MRI	2014	GLCM	-	SVM	93.00%
[36]	MRI	2015	Texture and shape	ICA	SVM	99.09%
[92]	MRI	2015	Wavelet	-	SVM	97.00%
[28]	MRI	2017	Texture and shape	-	SVM	97.10%
[93]	MRI	2017	Intensity and texture	-	ANN	92.43%
[97]	MRI	2020	DWT	Mean and standard deviation	DNN	95.8%

MRI Brain Tumor Classification Using DL

Difficulties remain in categorizing brain cancers from an MRI scan, despite encouraging developments in the field of ML algorithms for the classification of brain tumors into their different types. These difficulties are mostly the result of the ROI detection; typical labor-intensive feature extraction methods could be more effective [33]. Owing to the nature of deep learning, the categorization of brain tumors is now a data-driven problem rather than a challenge based on manually created features [34]. CNN is one of the deep learning models that is frequently utilized in brain tumor classification tasks and has produced a significant result [35].

According to a study [101], the CNN algorithm can be used to divide the severity of gliomas into two categories: low severity or high severity, as well as multiple grades of severity (Grades II, III, and IV). Accuracy rates of 71% and 96% were reached by the classifier.

A DL approach based on a CNN was proposed by Sultan et al. [7] to classify different kinds of brain tumors using two publicly available datasets. The proposed method's block diagram is presented in Figure 7 The first divides cancers into meningioma, pituitary, and glioma tumors. The other one distinguishes among Grade II, III, and IV gliomas. The first and second datasets, which each have 233 and 73 patients, contain a combined total of 3064 and 516 T1 images. The suggested network configuration achieves the best overall accuracy, 96.13% and 98.7%, for the two studies, which results in significant performance [7].

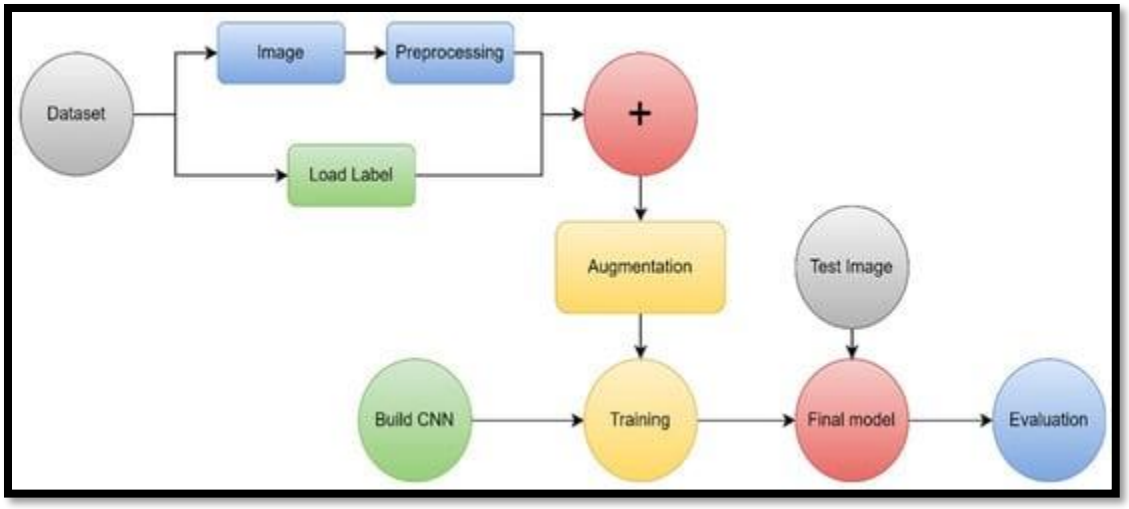

Figure 7. A block schematic showing the suggested approach. Reprinted (adapted) with permission from [7]. Copyright 2019 IEEE.

Similarly, ref. [36] showed how to classify brain MRI scan images into malignant and benign using CNN algorithms in conjunction with augmenting data and image processing. They evaluated the effectiveness of their CNN model with pretrained VGG-16, Inception-v3, and ResNet-50 models using the transfer learning methodology. Even though the experiment was carried out on a relatively small dataset, the results reveal that the model's accuracy result is quite strong and has a very low complexity rate, as it obtained 100% accuracy, compared to VGG-16's 96%, ResNet-50's 89%, and Inception-V3's 75%. The structure of the suggested CNN architecture is shown in Figure 8

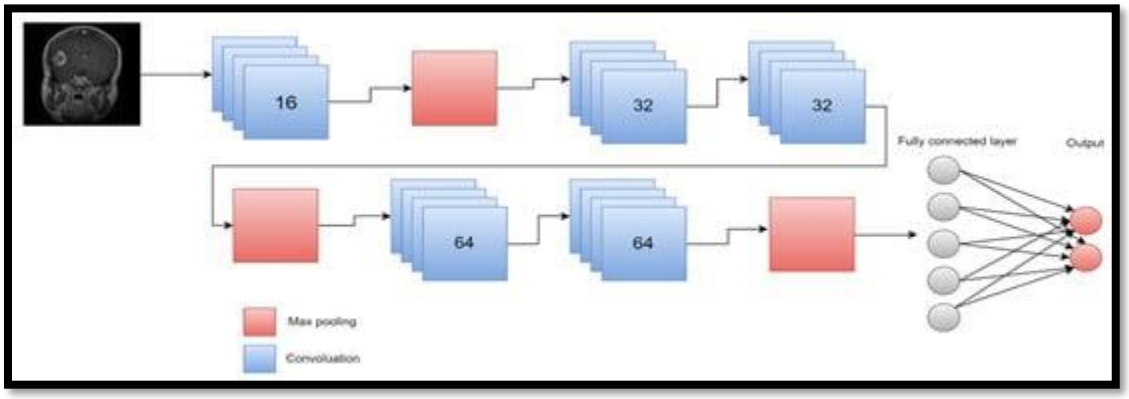

Figure 8. Proposed method. Reprinted (adapted) with permission from [37]. Copyright 2020 Mathematical Biosciences and Engineering.

For accurate glioma grade prediction, researchers developed a customized CNN-based deep learning model [38] and evaluated the performance using AlexNet, GoogleNet, and SqueezeNet by transfer learning. Based on 104 clinical glioma patients with (50 LGGs and 54 HGGs), they trained and evaluated the models. The training data was expanded using a variety of data augmentation methods. A five-fold cross-validation procedure was used to assess each model's performance. According to the study's findings, their specially created deep CNN model outperformed the pretrained models by an equal or greater percentage. The custom model's accuracy, sensitivity, F1 score, specificity, and AUC values were, respectively, 0.971, 0.980, 0.970, 0.963, and 0.989.

A novel transfer learning-based active learning paradigm for classifying brain tumors was proposed by Ruqian et al. [39]. Figure 9 describes the workflow for active learning. On the MRI training dataset of 203 patients and the baseline validation dataset of 66 patients, they used a 2D slice-based technique to train and fine-tune the model. Their suggested approach allowed the model to obtain an area under the curve (ROC) of 82.89%. The researchers built a balanced dataset and ran the same process on it to further investigate the robustness of their strategy. Compared to the baseline's AUC of 78.48%, the model's AUC was 82%.

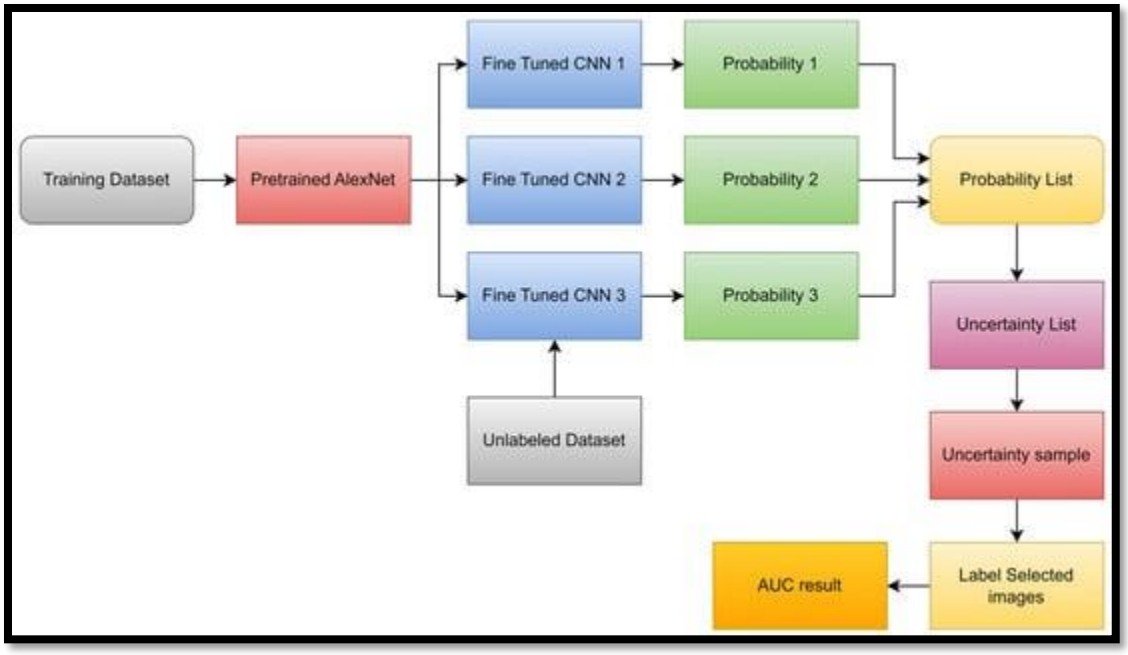

Figure 9 Workflow of the suggested active learning framework based on transfer learning. Reprinted (adapted) with permission from [104]. Copyright 2021 Frontiers in Artificial Intelligence.

A total of 131 patients with glioma were enrolled [39]. A rectangular ROI was used to segment tumor images, and this ROI contained around 80% of the tumor. The test dataset was then created by randomly selecting 20% of the patient-level data. Models previously trained on the expansive natural image database ImageNet were applied to MRI images, and then AlexNet and GoogleNet were developed from scratch and fine-tuned. Five-fold cross-validation (CV) was used on the patient-level split to evaluate the classification task. The averaged performance metrics for validation accuracy, test accuracy, and test AUC from the five-fold CV of GoogleNet were, respectively, 0.867, 0.909, and 0.939.

Hamdaoui et al. [40] proposed an intelligent medical decision-support system for identifying and categorizing brain tumors using images from the risk of

malignancy index. They employed deep transfer learning principles to avoid the scarcity of training data required to construct the CNN model. For this, they selected seven CNN architectures that had already been trained on an ImageNet dataset that they carefully fitted on (MRI) data of brain tumors gathered from the BRATS database, as shown in Figure 10. Just the prediction that received the highest score among the predictions made by the seven pretrained CNNs is produced to increase their model's accuracy. They evaluated the effectiveness of the primary two-class model, which includes LGG and HGG brain cancers, using a ten-way cross-validation method. The test precision, F1 score, test precision, and test sensitivity for their suggested model were 98.67%, 98.06%, 98.33%, and 98.06%, respectively.

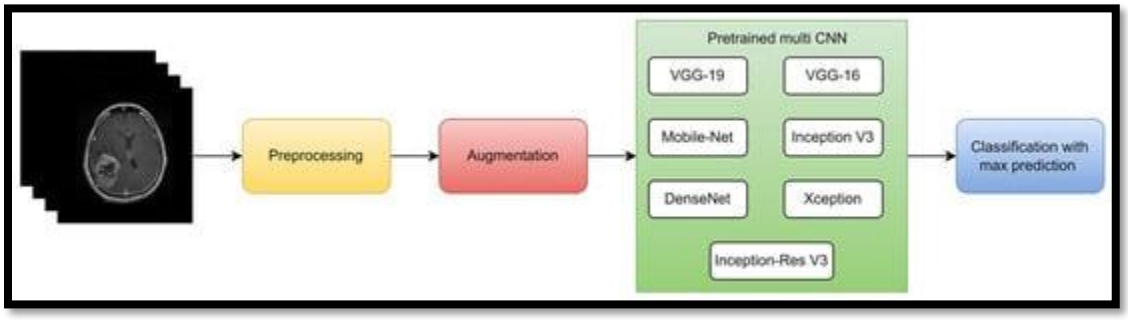

Figure 10. Proposed process for deep transfer learning. Reprinted (adapted) with permission from [41]. Copyright 2021 Indonesian Journal of Electrical Engineering and Computer Science.

A new AI diagnosis model called EfficientNetB0 was created by Khazaee et al. [42] to assess and categorize human brain gliomas utilizing sequences from MR images. They used a common dataset (BRATS-2019) to validate the new AI model, and they showed that the AI components—CNN and transfer learning—provided

outstanding performance for categorizing and grading glioma images, with 98.8% accuracy.

In [43], the researchers developed a model using transfer learning and pretrained ResNet18 to identify basal ganglia germinomas more accurately. In this retrospective analysis, 73 patients with basal ganglioma were enrolled. Based on both T1 and T2 data, brain tumors were manually segmented. To create the tumor classification model, the T1 sequence was utilized. Transfer learning and a 2D convolutional network were used. Five-fold cross-validation was used to train the model, and it resulted in a mean AUC of 88%.

Researchers suggested an effective hyperparameter optimization method for CNN based on Bayesian optimization [44]. This method was assessed by categorizing 3064 T1 images into three types of brain cancers (glioma, pituitary, and meningioma). Five popular deep pretrained models are compared to the improved CNN's performance using transfer learning. Their CNN achieved 98.70% validation accuracy after applying Bayesian optimization.

A novel generated transfer DL model was developed by Alanazi et al. [45] for the early diagnosis of brain cancers into their different categories, such as meningioma, pituitary, and glioma. Several layers of the models were first constructed from scratch to test the performance of standalone CNN models performed for brain MRI images. The weights of the neurons were then revised using the transfer learning approach to categorize brain MRI images into tumor subclasses using the 22-layer, isolated CNN model. Consequently, the transfer-learned model that was created had an accuracy rate of 95.75%.

Rizwan et al. [45] suggested a method to identify various BT classes using Gaussian-CNN on two datasets. One of the datasets is employed to categorize

lesions into pituitary, glioma, and meningioma. The other distinguishes between the three glioma classes (II, III, and IV). The first and second datasets, respectively, have 233 and 73 victims from a total of 3064 and 516 images on T1 enhanced images. For the two datasets, the suggested method has an accuracy of 99.8% and 97.14%.

A seven-layer CNN was suggested in [46] to assist with the three-class categorization of brain MR images. To decrease computing time, separable convolution was used. The suggested separable CNN model achieved 97.52% accuracy on a publicly available dataset of 3064 images.

Several pretrained CNNs were utilized in [47], including GoogleNet, Alexnet, Resnet50, Resnet101, VGG-16, VGG-19, InceptionResNetV2, and Inceptionv3. To accommodate additional image categories, the final few layers of these networks were modified. Data from the clinical, Harvard, and Figshare repositories were widely used to assess these models. The dataset was divided into training and testing halves in a 60:40 ratio. The validation on the test set demonstrates that, compared to other proposed models, the Alexnet with transfer learning demonstrated the best performance in the shortest time. The suggested method obtained accuracies of 100%, 94%, and 95.92% using three datasets and is more generic because it does not require any manually created features.

The suggested framework [48] describes three experiments that classified brain malignancies such as meningiomas, gliomas, and pituitary tumors using three designs of CNN (AlexNet, VGGNet, and GoogleNet). Using the MRI slices of the brain tumor dataset from Figshare, each study then investigates transfer learning approaches like fine-tuning and freezing. The data augmentation approaches are applied to the MRI slices for results generalization, increasing dataset samples, and

minimizing the risk of overfitting. The fine-tuned VGG16 architecture attained the best accuracy at 98.69% in terms of categorization in the proposed studies.

An effective hybrid optimization approach was used in [49] for the segmentation and classification of brain tumors. To improve categorization, the CNN features were extracted. The suggested chronological Jaya honey badger algorithm (CJHBA) was used to train the deep residual network (DRN), which was used to conduct the classification by using the retrieved features as input. The Jaya algorithm, the honey badger algorithm (HBA), and the chronological notion are all combined in the proposed CJHBA. Using BRATS-2018, the performance is assessed. The highest accuracy is 92.10%. A summary of MRI brain tumor classification using DL is provided in Table 4.

Table 4. MRI brain tumor classification using DL.

Ref.	Scan	Year	Technique	Method	Result	Performance Metrics
[101]	MRI	2015	DL	Custom-CNN	96.00%	Acc
[7]	MRI	2019	DL	Custom-CNN	98.70%	Acc
[102]	MRI	2020	DL	VGG-16, Inception-v3, ResNet-50	96% 75% 89%	Acc
[103]	MRI	2021	DL	AlexNet, GoogleNet, SqueezeNet	97.10%	Acc
[104]	MRI	2021	DL	Custom-CNN	82.89%	ROC
[105]	MRI	2018	DL	AlexNet	90.90%	Test acc
[106]	MRI	2021	DL	multi-CNN structure	98.67% 98.06% 98.33% 98.06%	precision, F1 score, precision, sensitivity
[107]	MRI	2022	DL	EfficientNetB0	98.80%	Acc
[70]	MRI	2022	DL	ResNet18	88.00%	AUC
[108]	MRI	2022	DL	Custom-CNN	98.70%	Acc
[109]	MRI	2022	DL	Custom-CNN	95.75%	Acc

[110]	MRI	2022	DL	Gaussian-CNN	99.80%	Acc
[111]	MRI	2020	DL	seven-layer CNN	97.52%	Acc
[112]	MRI	2021	DL	Alexnet	100.00%	Acc
[113]	MRI	2019	DL	VGG16	98.69%	Acc
[114]	MRI	2023	DL	CNN	92.10%	Acc

2.11. X-rays

X-rays (in English: It ranges from 124 electronvolts to 124 kiloelectronvolts. X-rays are widely used in radiography and in many technical and scientific fields. It was discovered by the German scientist William Roentgen in 1895 at the University of Würzburg, and won the Nobel Prize in Physics in 1901. (50)

William Roentgen, the discoverer of X-rays, shone an electron beam into a glass tube with high electrical tension between its ends. This was a vacuum tube, and electrons inside it traveled from a negative electrode to a positive electrode. This tube was surrounded by light-colored paper to protect the user from the emitted electromagnetic field, and a phosphorescent screen was placed at the end. When the electron beam hit the screen, it began to glow. When Richard Roentgen accidentally put his hand between the tube and the phosphorescent screen, he saw an image of his hand bones on the screen. This was the first X-ray imaging process (52)

2.12. uses

are radiography in medicine to detect teeth and bones and their fractures, determine the location of solid objects such as shrapnel or bullets in the body, as well as detect tumors in the body. Thanks to these rays, it has become possible to

see bone fractures with high accuracy, as these rays can penetrate soft objects such as skin, but they do not You can pass through the bones, causing an image of the latter to appear. One of its most important features is its lack of side effects.(53)

Doctors also use these rays to treat and eliminate cancerous tumors. X-rays kill and eliminate cancer cells, while healthy body cells regain their vitality after a short period and return healthy. (54)

X-rays were also used in industry to detect dents and cracks in metal molds and wood used in the manufacture of boats. Studying the absorption spectrum of these rays in matter also helped make X-rays a method for detecting and analyzing the elements involved in the composition of various materials. In this case, X-rays are used to distinguish each chemical element. It has become possible to measure the thickness of solid materials and scan industrial parts for defects that cannot be observed with the naked eye using these rays.(55)

In the field of security, X-rays are used to monitor passengers' bags at airports in search of weapons or bombs In the science of studying solid bodies, using X-ray diffraction it became clear that there is a certain symmetry in some types of solids (crystals), and this was the beginning of a huge breakthrough in studying the properties of solids and crystal structure, and knowing the atomic structure of the elements.(56)

In the field of art, it has been used to identify painters' methods and distinguish between real paintings and fake paintings. This is because the colors used in ancient paintings contain many metallic compounds that absorb X-rays, while the colors used in modern paintings are organic compounds that absorb X-rays to a lesser extent.(57)

The aim of study

Learn about the CT device and how it works, and learn about its parts and components.

Chapter Three

literature review

1. **Automatic exposure control in CT: an investigation between different manufacturers considering radiation dose and image quality.** Marcus Söderberg Supervisor: Mikael Gunnarsson, PhD.

Data from 1998 showed that CT represents about 10% of all the diagnostic X-ray examinations and almost 70% of the total radiation dose from medical diagnostic examinations in Sweden. Because of this there is a strong need to minimize the radiation dose and adapt the dose to each patient's examination area and anatomy. Today practically all-modern CT systems are delivered with automatic exposure control (AEC) systems that perform tube current modulation in 3D.

2. ESTIMATION OF BREAST DOSE AND CANCER RISK IN CHEST AND ABDOMEN CT PROCEDURES by: Suha Abubaker, Ali Eltahir United Arab Emirates University 2008

The use of CT in medical diagnosis delivers radiation doses to patients that are higher than those from other radiological procedures. Lack of optimized protocols could be an additional source of increased dose in developing countries. The aims of this study are, first, to measure patient doses during CT chest and abdomen procedures, second, to estimate the radiation dose to the breast, and third, to quantify the radiation risks during the procedures.Patient doses from two common CT examinations were obtained from four hospitals in Khartoum. The patient doses were estimated using measurements of CT dose indexes (CTDI), exposure-related parameters, and the ImPACT spreadsheet based on NRPB conversion factors. A large variation of mean organ doses among hospitals was observed for

similar CT examinations. These variations largely originated from different CT scanning protocols used in different hospitals and scanner type.

3. **Lithuanian University of Health Sciences Faculty of Medicine Mohammad Asif Malik :** This was a Systematic Literature review where searches were conducted using several databases: Medline (PubMed), science direct publications and UpToDate. All articles published from 2008 were included in the searches with no more than 10 years search criteria used. The search terms used were: 'cardiac CT,' 'cardiac CT in the emergency setting,' 'CT angiography in the emergency settings,' 'calcium score in emergency settings,' 'Triple rule out in emergency settings.' Keywords were matched to database indexing terms. In PubMed, the related articles were also retrieved and added to this review.

4**. Anatomically Constrained Image Reconstruction applied to Emission Computed Tomography & Magnetic Impedance Tomography ; Robert Henry** Ireland Anatomically Constrained Image Reconstruction applied to Emission Computed Tomography and Magnetic Impedance Tomography Rob Ireland, Department of Medical Physics & Clinical Engineering The University of Sheffield, UK Multimodality medical imaging provides useful diagnostic anatomical and functional information. In certain cases, functional image reconstruction can be improved by the incorporation of a priori anatomical information. The aim of this thesis is to investigate methods of using high resolution anatomical images to constrain the reconstruction of lower resolution functional images.

5. **Applying Computed Tomography (CT) scanning for segmentation of permafrost constituents in drill cores** , Damir Gadylyaev Computed X-ray Tomography is a non-destructive technique that allows three-dimensional imaging

of soil samples' internal structures, deter mined by their density and atomic composition variations. The objective of this thesis is to develop an image processing work ow for the quan titative analysis of ice cores using high-resolution CT to determine the volume fraction and vertical distribution of ice, mineral, gas, and organic matter in permafrost cores. I analyzed a 164 cm permafrost core taken from a Yedoma permafrost upland on Kurungnakh Island in the Lena River Delta (northeast Siberia). The obtained results were evaluated and compared with the results of detailed but sample-destructive laboratory analysis. The frozen permafrost core was subjected to a computerized X-ray imaging procedure with a resolution of 50 micrometers.

Chapter three

Patient and materials

Patient and materials

Components of a CT scan machine

3.1. CT scan room design

Most of the components of the CT scan device are located inside the gantry. In addition to the gantry, the CT scan device also consists of an examination table and a control room. The design of CT scan rooms is usually similar, in that the examination table and gantry are in a room, while the control room is outside behind a lead barrier to protect against radiation. (58)

In the control room there is a special computer that the radiology technician works on at the time of imaging, and part of the wall must be a window made of lead-equivalent glass so that we can see inside the room to intervene in the event of any emergency. The entrance for patients is different from the entrance for radiology technicians for several reasons, the most important of which are: protection from infection and so that it cannot be opened from the outside to ensure that no one enters at the time of radiation. It must also be a wide entrance to suit the patients' beds. It is important to have a waiting room and a changing room, and it is also possible to provide lockers for patients' belongings.(59)

3.2. Generator

.Modern high-frequency generators are small in size so that they can be placed inside the gantry. Its function is to produce electrical energy and send it to the x-ray tube. (60)

3.3. X-ray tube

The function of the x-ray tube is to generate x-rays (61)

3.4. **Filtration**

Using a filter improves image quality and reduces the radiation dose to the patient. The filter absorbs radiation photons of weak energy that will certainly be absorbed in the patient's body and will not reach the radiation receiver. These photons will not contribute to the image, but will increase the radiation dose to the patient.(62)

3.5.**Collimators**

The function of the collimator is to determine the radiation field and this leads to reducing scatter radiation. By reducing scatter, the image quality improves and the radiation dose to the patient is reduced. The collimator controls the thickness of the CT scan image by expanding or decreasing the radiation field based on the choice of the radiology technician. (63)

Figer (11) images from a CT scan





Figer (11)A

Figer (11) B

3.6. GoldSeal Certified GE LightSpeed RT Series

Refurbished LightSpeed RT products are multi-slice CT systems optimized for CT simulation in your Radiation Oncology department.

3.7. Overview Precision at an Affordable Price

Radiotherapy simulation and planning demand the accuracy and precision of CT systems like the LightSpeed RT family. GoldSeal LightSpeed RT4 and RT16 systems help you image small structures, and see fine details for accurate contouring, and accurately detect edges of tumors in motion. The result is an effective balance of resolution, coverage, speed and dose for radiation therapy simulation at its best.

- LightSpeed RT 4 delivers thin, multi-slice imaging that enables retrospective respiratory gating and improved target delineation.
- LightSpeed RT 16 provides routine 16-slice acquisition with outstanding image clarity and 20mm of coverage.

3.8.Benefits

The LightSpeed RT4 and LightSpeed RT16 provide for:

- Accurate 3D visualization
- Fast scan times to improve productivity
- Optimized workflow from acquisition to final report
- Increased patient comfort with faster scans
- Precise positioning of patients even in challenging cases

3.9.Technology

. LightSpeed RT4 is a 4-slice per rotation multi-slice CT scanner; LightSpeed RT16 provides routine 16-slice acquisition. In addition, the LightSpeed RT Series of CT scanners include: Xtream* technology Breathing lights with countdown timer In-room start Slip-ring technology with advanced axial scanning Full 360º rotational scans Natural, intuitive user interface Remote gantry tilt.

3.10.Specifications

- GoldSeal LightSpeed RT Series scanner specifications include: 80 cm-gantry opening
- 65cm-wide display field of view

3.11.GoldSeal Advantage

GoldSeal pre-owned, refurbished systems offer you a smart use of resources, as well as:

- Selective process: Stringent selection standards ensure that only those systems with well-known and acceptable service histories qualify for GoldSeal.
- Quality: Refurbishing completed by OEM factory-trained technicians who ensure all OEM specifications are met.
- Same-as-new warranty: Same one-year warranty as on new systems; service contracts available.
- Service/support: Online assistance with questions, local service.
- Up-to-date technology: Refurbishing includes installation of latest possible software release and original OEM parts.
- Training: Operation and application training available, with optional CE Tech training credits available.

Figer (12) A collection of images from a CT scan with images of a brain scan.



Figer (12)A



Figer (12)B



Figer (12)C



Figer (12)D



Figer (12)E



Figer (12)F

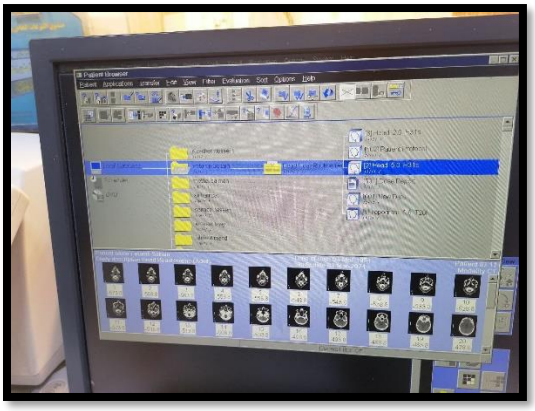

Figer (12)G

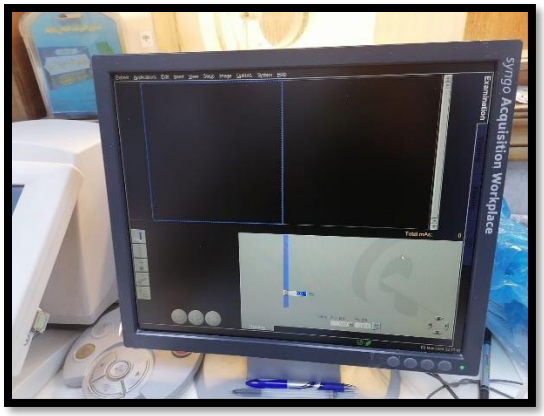

Figer (12)H



Figer (12)I



Figer (12)J

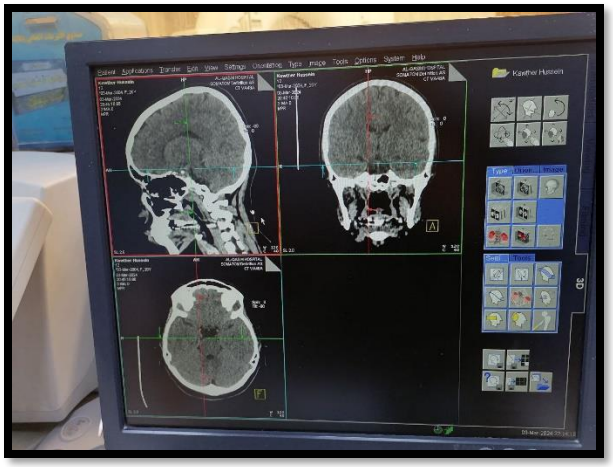

Figer (12)K

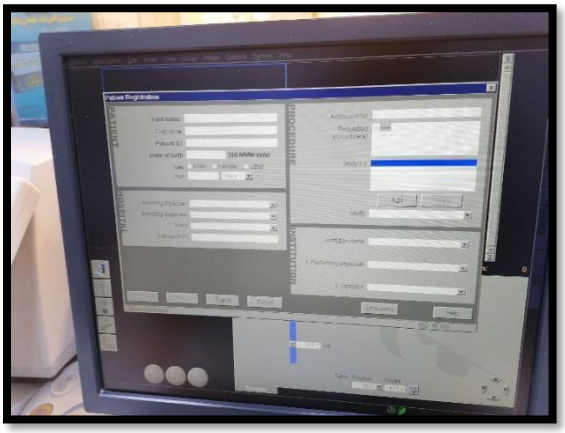

Figer (12)L

Chapter four

Discussion

4.1. Discussion

A brain tumor is an abnormal growth of brain tissue that affects the brain's ability to function normally. The primary objective in medical image processing is to find accurate and helpful information with the minimum possible errors by using algorithms. The four steps involved in segmenting and categorizing brain tumors using MRI data are preprocessing, picture segmentation, extracting features, and image classification. The diagnosis, treatment strategy, and patient follow-up can all be greatly enhanced by automating the segmentation and categorization of brain tumors. It is still difficult to create a fully autonomous system that can be deployed on clinical floors due to the appearance of the tumor and its irregular size, form, and nature. The review's primary goal is to present the state-of-the-art in the field of brain cancer, which includes the pathophysiology of the disease, imaging technologies, WHO classification standards for tumors, primary methods of diagnosis, and CAD algorithms for brain tumor classifications using ML and DL techniques. Automating the segmentation and categorization of brain tumors using deep learning techniques has many advantages over region-growing and shallow ML systems. DL algorithms' powerful feature learning capabilities are primarily to blame for this. Although DL techniques have made a substantial contribution, a general technique is still needed. This study reviewed 53 studies that used ML and DL to classify brain tumors based on MRI, and it examined the challenges and obstacles that CAD brain tumor classification techniques now face in practical application and advancement—a thorough examination of the variables that might impact classification accuracy. The MRI sequences and web address of the online repository for the dataset are among the publicly available databases that have been briefly listed in Table 4 and used in the experiments evaluated in this paper.

4.2. Conclusion

The reconstruction of tomographic medical images constitutes an ill-posed inverse problem. The need to impose a priori knowledge of the form of the desired solution has long been recognised and the use of structural or anatomical constraints is a natural extension to previous, well-developed techniques. Regularisation with anatomical information not only reduces the influence of noise but also improves the distinction of boundaries between tissue type and anatomical regions, thereby raising the possibility of correcting for the partial volume effect for example.

In this thesis, the concept of anatomically constrained functional image reconstruction has been reviewed and new theoretical methods for relatively high and low functional imaging modalities have been proposed. Looking forward, it is reasonable to speculate. that the proliferation of hybrid imaging systems may stimulate further research into multimodality image reconstruction that could result in the clinical use of anatomically constrained methods.

References

1. Watson, C.; Kirkcaldie, M.; Paxinos, G. The Brain: An Introduction to Functional Neuroanatomy. 2010. Available online: http://ci.nii.ac.jp/ncid/BB04049625 (accessed on 22 May 2023).

2. Jellinger, K.A. The Human Nervous System Structure and Function, 6th edn. *Eur. J. Neurol.* 2009, *16*, e136. [Google Scholar] [CrossRef]

3. DeAngelis, L.M. Brain tumors. *N. Engl. J. Med.* 2001, *344*, 114–123. [Google Scholar] [CrossRef]

4. Louis, D.N.; Perry, A.; Wesseling, P.; Brat, D.J.; Cree, I.A.; Figarella-Branger, D.; Hawkins, C.; Ng, H.K.; Pfister, S.M.; Reifenberger, G.; et al. The 2021 WHO Classification of Tumors of the Central Nervous System: A summary. *Neuro-Oncology* 2021, *23*, 1231–1251. [Google Scholar] [CrossRef]

5. Hayward, R.M.; Patronas, N.; Baker, E.H.; Vézina, G.; Albert, P.S.; Warren, K.E. Inter-observer variability in the measurement of diffuse intrinsic pontine gliomas. *J. Neuro-Oncol.* 2008, *90*, 57–61. [Google Scholar] [CrossRef]

6. Mahaley, M.S., Jr.; Mettlin, C.; Natarajan, N.; Laws, E.R., Jr.; Peace, B.B. National survey of patterns of care for brain-tumor patients. *J. Neurosurg.* 1989, *71*, 826–836. [Google Scholar] [CrossRef] [PubMed]

7. Sultan, H.H.; Salem, N.M.; Al-Atabany, W. Multi-Classification of Brain Tumor Images Using Deep Neural Network. *IEEE Access* 2019, *7*, 69215–69225. [Google Scholar] [CrossRef]

8. Johnson, D.R.; Guerin, J.B.; Giannini, C.; Morris, J.M.; Eckel, L.J.; Kaufmann, T.J. 2016 Updates to the WHO Brain Tumor Classification System: What the Radiologist Needs to Know. *RadioGraphics* 2017, *37*, 2164–2180. [Google Scholar] [CrossRef] [PubMed]

9. Buckner, J.C.; Brown, P.D.; O'Neill, B.P.; Meyer, F.B.; Wetmore, C.J.; Uhm, J.H. Central Nervous System Tumors. *Mayo Clin. Proc.* 2007, *82*, 1271–1286. [Google Scholar] [CrossRef] [PubMed]

10. World Health Organization: WHO, "Cancer". July 2019. Available online: https://www.who.int/health-topics/cancer (accessed on 30 March 2022).

11. Amyot, F.; Arciniegas, D.B.; Brazaitis, M.P.; Curley, K.C.; Diaz-Arrastia, R.; Gandjbakhche, A.; Herscovitch, P.; Hinds, S.R.; Manley, G.T.; Pacifico, A.; et al. A Review of the Effectiveness of Neuroimaging Modalities for the Detection of Traumatic Brain Injury. *J. Neurotrauma* 2015, *32*, 1693–1721. [Google Scholar] [CrossRef]

12. Pope, W.B. Brain metastases: Neuroimaging. *Handb. Clin. Neurol.* 2018, *149*, 89–112. [Google Scholar] [CrossRef]

13. Abd-Ellah, M.K.; Awad, A.I.; Khalaf, A.A.; Hamed, H.F. A review on brain tumor diagnosis from MRI images: Practical implications, key achievements, and lessons learned. *Magn. Reson. Imaging* 2019, *61*, 300–318. [Google Scholar] [CrossRef] [PubMed]

14. Ammari, S.; Pitre-Champagnat, S.; Dercle, L.; Chouzenoux, E.; Moalla, S.; Reuze, S.; Talbot, H.; Mokoyoko, T.; Hadchiti, J.; Diffetocq, S.; et al. Influence of Magnetic Field Strength on Magnetic Resonance Imaging Radiomics Features in Brain Imaging, an In Vitro and In Vivo Study. *Front. Oncol.* 2021, *10*, 541663. [Google Scholar] [CrossRef] [PubMed]

15. Sahoo, L.; Sarangi, L.; Dash, B.R.; Palo, H.K. Detection and Classification of Brain Tumor Using Magnetic Resonance Images. In *Advances in Electrical Control and Signal Systems: Select Proceedings of AECSS, Bhubaneswar, India, 8–9 November 2019*; Springer: Singapore, 2020; Volume 665, pp. 429–441. [Google Scholar] [CrossRef]

16. Kaur, R.; Doegar, A. Localization and Classification of Brain Tumor using Machine Learning & Deep Learning Techniques. *Int. J. Innov. Technol. Explor. Eng.* 2019, *8*, 59–66. [Google Scholar]

17. The Radiology Assistant: Multiple Sclerosis 2.0. 1 December 2021. Available online: https://radiologyassistant.nl/neuroradiology/multiple-sclerosis/diagnosis-and-differential-diagnosis-3#mri-protocol-ms-brain-protocol (accessed on 22 May 2023).

18. Savoy, R.L. Functional magnetic resonance imaging (fMRI). In *Encyclopedia of Neuroscience*; Elsevier: Charlestown, MA, USA, 1999. [Google Scholar]

19. Luo, Q.; Li, Y.; Luo, L.; Diao, W. Comparisons of the accuracy of radiation diagnostic modalities in brain tumor. *Medicine* 2018, *97*, e11256. [Google Scholar] [CrossRef]

20. Positron Emission Tomography (PET). Johns Hopkins Medicine. 20 August 2021. Available online: https://www.hopkinsmedicine.org/health/treatment-tests-and-therapies/positron-emission-tomography-pet (accessed on 20 May 2023).

21. Mayfield Brain and Spine. SPECT Scan. 2022. Available online: https://mayfieldclinic.com/pe-spect.htm (accessed on 22 May 2023).

22. Sastry, R.; Bi, W.L.; Pieper, S.; Frisken, S.; Kapur, T.; Wells, W.; Golby, A.J. Applications of Ultrasound in the Resection of Brain Tumors. *J. Neuroimaging* 2016, *27*, 5–15. [Google Scholar] [CrossRef]

23. Nasrabadi, N.M. Pattern recognition and machine learning. *J. Electron. Imaging* 2007, *16*, 49901. [Google Scholar]

24. Erickson, B.J.; Korfiatis, P.; Akkus, Z.; Kline, T.L. Machine learning for medical imaging. *Radiographics* 2017, *37*, 505–515. [Google Scholar] [CrossRef]

25. Mohan, M.R.M.; Sulochana, C.H.; Latha, T. Medical image denoising using multistage directional median filter. In Proceedings of the 2015 International Conference on Circuits, Power and Computing Technologies [ICCPCT-2015], Nagercoil, India, 9–20 March 2015. [Google Scholar]

26. Borole, V.Y.; Nimbhore, S.S.; Kawthekar, S.S. Image processing techniques for brain tumor detection: A review. *Int. J. Emerg. Trends Technol. Comput. Sci. (IJETTCS)* 2015, *4*, 2. [Google Scholar]

27. Ziedan, R.H.; Mead, M.A.; Eltawel, G.S. Selecting the Appropriate Feature Extraction Techniques for Automatic Medical Images Classification. *Int. J.* 2016, *4*, 1–9. [Google Scholar]

28. Amin, J.; Sharif, M.; Yasmin, M.; Fernandes, S.L. A distinctive approach in brain tumor detection and classification using MRI. *Pattern Recognit. Lett.* 2017, *139*, 118–127. [Google Scholar] [CrossRef]

29. Islam, A.; Reza, S.M.; Iftekharuddin, K.M. Multifractal texture estimation for detection and segmentation of brain tumors. *IEEE Trans. Biomed. Eng.* 2013, *60*, 3204–3215. [Google Scholar] [CrossRef]

30. Gurbină, M.; Lascu, M.; Lascu, D. Tumor detection and classification of MRI brain image using different wavelet transforms and support vector machines. In Proceedings of the 2019 42nd International Conference on Telecommunications and Signal Processing (TSP), Budapest, Hungary, 1–3 July 2019; pp. 505–508. [Google Scholar]

31. Xu, X.; Zhang, X.; Tian, Q.; Zhang, G.; Liu, Y.; Cui, G.; Meng, J.; Wu, Y.; Liu, T.; Yang, Z.; et al. Three-dimensional texture features from intensity and high-order derivative maps for the discrimination between bladder tumors and wall tissues via MRI. *Int. J. Comput. Assist. Radiol. Surg.* 2017, *12*, 645–656. [Google Scholar] [CrossRef]

32. Kaplan, K.; Kaya, Y.; Kuncan, M.; Ertunç, H.M. Brain tumor classification using modified local binary patterns (LBP) feature extraction methods. *Med. Hypotheses* 2020, *139*, 109696. [Google Scholar] [CrossRef]

33. Afza, F.; Khan, M.S.; Sharif, M.; Saba, T. Microscopic skin laceration segmentation and classification: A framework of statistical normal distribution and optimal feature selection. *Microsc. Res. Tech.* 2019, *82*, 1471–1488. [Google Scholar] [CrossRef]

34. Lakshmi, A.; Arivoli, T.; Rajasekaran, M.P. A Novel M-ACA-Based Tumor Segmentation and DAPP Feature Extraction with PPCSO-PKC-Based MRI Classification. *Arab. J. Sci. Eng.* 2017, *43*, 7095–7111. [Google Scholar] [CrossRef]

35. Adair, J.; Brownlee, A.; Ochoa, G. Evolutionary Algorithms with Linkage Information for Feature Selection in Brain Computer Interfaces. In *Advances in Computational Intelligence Systems*; Springer Nature: Cham, Switzerland, 2016; pp. 287–307. [Google Scholar]

36. Arakeri, M.P.; Reddy, G.R.M. Computeraided diagnosis system for tissue characterization of brain tumor on magnetic resonance images. *Signal Image Video Process.* 2015, *9*, 409–425. [Google Scholar] [CrossRef]

37. Wang, S.; Zhang, Y.; Dong, Z.; Du, S.; Ji, G.; Yan, J.; Phillips, P. Feed-forward neural network optimized by hybridization of PSO and ABC for abnormal brain detection. *Int. J. Imaging Syst. Technol.* 2015, *25*, 153–164. [Google Scholar] [CrossRef]

38. Abbasi, S.; Tajeripour, F. Detection of brain tumor in 3D MRI images using local binary patterns and histogram orientation gradient. *Neurocomputing* 2017, *219*, 526–535. [Google Scholar] [CrossRef]

39. Zöllner, F.G.; Emblem, K.E.; Schad, L.R. SVM-based glioma grading: Optimization by feature reduction analysis. *Z. Med. Phys.* 2012, *22*, 205–214. [Google Scholar] [CrossRef]

40. Huang, G.-B.; Zhu, Q.-Y.; Siew, C.-K. Extreme learning machine: Theory and applications. *Neurocomputing* 2006, *70*, 489–501. [Google Scholar] [CrossRef]

41. Bhatele, K.R.; Bhadauria, S.S. Brain structural disorders detection and classification approaches: A review. *Artif. Intell. Rev.* 2019, *53*, 3349–3401. [Google Scholar] [CrossRef]

42. Schmidhuber, J. Deep Learning in Neural Networks: An Overview. *Neural Netw.* 2015, *61*, 85–117. [Google Scholar] [CrossRef]

43. Hu, A.; Razmjooy, N. Brain tumor diagnosis based on metaheuristics and deep learning. *Int. J. Imaging Syst. Technol.* 2020, *31*, 657–669. [Google Scholar] [CrossRef]

44. Tandel, G.S.; Balestrieri, A.; Jujaray, T.; Khanna, N.N.; Saba, L.; Suri, J.S. Multiclass magnetic resonance imaging brain tumor classification using artificial intelligence paradigm. *Comput. Biol. Med.* 2020, *122*, 103804. [Google Scholar] [CrossRef] [PubMed]

45. Sahaai, M.B. Brain tumor detection using DNN algorithm. *Turk. J. Comput. Math. Educ. (TURCOMAT)* 2021, *12*, 3338–3345. [Google Scholar]

46. Hashemi, M. Enlarging smaller images before inputting into convolutional neural network: Zero-padding vs. interpolation. *J. Big Data* 2019, *6*, 98. [Google Scholar] [CrossRef]

47. Miotto, R.; Wang, F.; Wang, S.; Jiang, X.; Dudley, J.T. Deep learning for healthcare: Review, opportunities and challenges. *Briefings Bioinform.* 2017, *19*, 1236–1246. [Google Scholar] [CrossRef]

48. Gorach, T. Deep convolutional neural networks—A review. *Int. Res. J. Eng. Technol. (IRJET)* 2018, *5*, 439. [Google Scholar]

49. Ogundokun, R.O.; Maskeliunas, R.; Misra, S.; Damaševičius, R. Improved CNN Based on Batch Normalization and Adam Optimizer. In Proceedings of the Computational Science and Its Applications–ICCSA 2022 Workshops, Malaga, Spain, 4–7 July 2022; Part V. pp. 593–604. [Google Scholar]

50. "JOHN HALL-EDWARDS". Engole the Elven for Knowledge. 15 June 2018. Retrieved 27 October 2023.

51. Stoddart C (1 March 2022). "Structural biology: How proteins got their close-up". Knowable Magazine. Doi:10.1146/knowable-022822-1. Retrieved 25 March 2022.

52. Birmingham City Council: Major John Hall-Edwards Archived September 28, 2012, at the Wayback Machine

53. "X-ray movies show hard boiled egg fighting digestive organs (1913)". The News-Palladium. 4 April 1913. P. 2. Retrieved 26 November 2020.

54. "X-ray moving pictures latest (1913)". Chicago Tribune. 22 June 1913. P. 32. Retrieved 26 November 2020.

55. "Homeopaths to show movies of body's organs at work (1915)". The Central New Jersey Home News. 10 May 1915. P. 6. Retrieved 26 November 2020.

56. "X-ray movies perfected. Will show motions of bones and joints of human body. (1918)". The Sun. 7 January 1918. P. 7. Retrieved 26 November 2020.

57. "Talk is cheap? X-ray used by Institute of Phonetics (1920)". New Castle Herald. 2 January 1920. P. 13. Retrieved 26 November 2020.

58. Jorgensen TJ (10 October 2017). "Marie Curie and her X-ray vehicles' contribution to World War I battlefield medicine". The Conversation. Retrieved 23 February 2018.

59. "X-Rays for Fitting Boots". Warwick Daily News (Qld.: 1919–1954). 25 August 1921. P. 4. Retrieved 27 November 2020.

60. Hermena S, Young M (2022), "CT-scan Image Production Procedures", StatPearls, Treasure Island (FL): StatPearls Publishing, PMID 34662062, retrieved 2023-11-24

61. "Patient Page". ARRT – The American Registry of Radiologic Technologists. Archived from the original on 9 November 2014.

62. "Individual State Licensure Information". American Society of Radiologic Technologists. Archived from the original on 18 July 2013. Retrieved 19 July 2013.

63. Terrier F, Grossholz M, Becker CD (2012-12-06). Spiral CT of the Abdomen. Springer Science & Business Media. P. 4. ISBN 978-3-642-56976-0.